Research Paper

Effects of Zerumbone Combined with Paclitaxel on Molecules Related to Immunogenic Cell Death of Human Salivary Gland Mucoepidermoid Carcinoma Cells

GUIXIN LI[1], PENGCHENG HUANG, LIJUAN GUO[2], YUQI ZENG[1], LI GUAN[1], YIXUAN ZHU[1] AND SEN YANG[1]*

Department of Stomatology, Southwest Medical University, Luzhou, Sichuan Province 626000, [1]Department of Stomatology, [2]Department of Medicine, Suining Central Hospital, Suining, Sichuan Province 629000, People's Republic of China

To investigate the effects of zerumbone and paclitaxel on immunogenic cell death in human salivary gland mucoepidermoid carcinoma MC-3 cell line. The MC-3 cell line of mucoepidermoid carcinoma was selected for culturing, and the viability of MC-3 was detected by the cell counting kit-8 method, and the concentration of zerumbone was screened for the half inhibition rate of zerumbone in MC-3 cell line at half-maximal inhibitory concentration. The apoptosis rate was detected by flow apoptosis method; calreticulin and transmembrane glycoprotein cluster of differentiation 47 were detected by immunofluorescence method and flow cytometry. High mobility group protein B1 was detected by *in situ* hybridization. Zerumbone acted for 48 h at a concentration of 40 µmol/l to reach half-maximal inhibitory concentration ($p<0.01$). Zerumbone promoted MC-3 apoptosis as well as inhibited MC-3 proliferation and migration, and its effect was enhanced when combined with paclitaxel ($p<0.05$). Zerumbone induced an increase in the expression of calreticulin and high mobility group box 1 in the molecules associated with MC-3 immunogenic death ($p<0.01$), and the adenosine triphosphate content was elevated ($p<0.05$), and enhanced its effect when combined with paclitaxel ($p<0.05$). Zerumbone induced attenuation of cluster of differentiation 47 expression in MC-3 immunogenic death-related molecules ($p<0.05$), and the attenuation effect was not enhanced when combined with paclitaxel. Zerumbone can promote MC-3 apoptosis and inhibit its proliferation and migration, and its effects are enhanced in combination with paclitaxel. Zerumbone can induce immunogenic cell death in salivary gland mucoepidermoid carcinoma cells by affecting the levels of damage-related molecules, calreticulin, cluster of differentiation 47, adenosine triphosphate, and high mobility group box 1, and the ability of flower zerumbone and paclitaxel in salivary gland mucoepidermoid carcinoma lines to induce immunogenic cell death was enhanced when the combination of both was administered.

Key words: Carcinoma, mucoepidermoid, salivary gland neoplasms, immunogenic cell death, immunotherapy

Mucoepidermoid Carcinoma (MEC) is the most common salivary malignancy of the salivary gland. The diseased age is 55 y old, and it is the most common malignancy of the salivary glands in young people[1,2]. The latest version of the World Health Organization classification of head and neck tumors classifies salivary gland tumors, of which MEC is the histological subtype of the most common salivary gland malignancies[3]. The traditional treatment of dermoid carcinoma MEC is surgical treatment, but when there is perineural invasion, vascular and lymphatic vessel involvement, advanced high-grade malignancy, positive resection margin, and extraglandular expansion, the clinical guidelines for the treatment of head and neck tumors (National Comprehensive Cancer Network (NCCN), Head and Neck Cancers Guidelines) recommend chemo radiation to prolong their survival[4-6]. However, related studies show that the traditional transformation of the process treatment drugs, such as cisplatin Vinorelbine (VNB) regimen, Paclitaxel (PTX) and other term drugs, can prolong their survival, but often cause toxic reactions such as leukopenia and cytopenia granulosa. At the same time, due to drug resistance, conventional chemotherapy often affects the later stage of patients' curative effect[7-11].

The immunogenic death of tumors is increasingly studied, which reveals the prospect of various forgotten

***Address for correspondence**
E-mail: ys13880435413@163.com

Regulated Cell Death (RCD) patterns and clarifies its immunogenic properties[12]. Chemotherapy, radiation therapy, and targeted anticancer drugs can induce the release and exposure of immune-related molecules on the surface of tumor cells, enabling the immunogenicity of tumor cells. These immunogenic antigen molecules are collectively referred to as Damage Associated Molecule Patterns (DAMPs). Immunogenic Cell Death (ICD), the associated DAMPs include surface-exposed Calreticulin (CRT), the High Mobility Group Box 1 (HMGB1), Adenosine Triphosphate (ATP), integrin-related protein Cluster of Differentiation 47 (CD47), etc.,[13]. Natural compounds have become ICD inducers in recent studies new entry point[14], compared to traditional ICD inducers such as anthracycline, cisplatin and radiotherapy[15], because of its low side effects has become the focus of research. Zerumbone (ZER) is a sesquiterpene isolated from red ball ginger, with aging agent, antibacterial, antipyretic, anti-inflammatory, and immune regulation. Due to the mild toxic side effects of flower ginger sterone, its antitumor effects are gradually explored, including the inhibition of proliferation, angiogenesis and promoting apoptosis[16]. Recently, ZER inhibited the migration and death of oral MEC in suppressing salivary gland tumors. PTX, also derived from natural plants, has been shown to induce immunogenic death of tumor cells and release DAMPs[17,18]. However, MEC patients often have different degrees of side effects and MEC, showing moderate adaptability and some resistance to PTX[7]. Therefore, a series of experimental methods were used to investigate whether ZER could induce immunogenic death in human salivary gland MEC, and to detect the changes of DAMPs after combining a certain concentration of ZER and PTX on mucoepidermoid cancer cells.

MATERIALS AND METHODS

Cells:

Human salivary gland MEC cell line of MC3 cells were established and provided by the Oral Biology Section of the Military Medical University of the People's Liberation Army (PLA) air force.

Reagents:

Dulbecco's Modified Eagle Medium (DMEM)/F-12 (1:1) medium was purchased from Shanghai Yuanpei Biotechnology Co. Ltd.; fetal calf serum (Fetal Bovine Serum (FBS)) purchased from Nanjing Shenghang Biotechnology Co. Ltd., penicillin-streptomycin-gentamicin mixed solution (100X triantibody), 3,3′-Diaminobenzidine (DAB) color development kit, trypsin were purchased from Biosharp Biotechnology Co. Ltd., Dimethyl Sulfoxide (DMSO) purchase from Shanghai Biotechnology Biological Engineering Co. Ltd., Phosphate Buffer Solution (PBS) from Fuzhou Meixin Company; ZER purchased from Chengdu Letian Pharmaceutical Technology Co. Ltd., Cell Counting Kit-8 (CCK-8) test kit was purchased from APEX-BIO Biotechnology Co. Ltd., Annexin V-Fluorescein Isothiocyanate (FITC)/Propidium Iodide (PI) apoptosis detection kit was purchased from Suzhou Si Zhengbai Biotechnology Co. Ltd., rabbit monoclonal antibody to CRT (rabbit anti-CRT antibody), Alexa Fluor 488-labeled anti-rabbit Immunoglobulin G (IgG) H+L (goat anti-rabbit IgG H+L/AF488), and Alexa Fluor 594-labeled anti-rabbit IgG H+L (goat anti-rabbit IgG H+L/AF594) were purchased from Beijing Boosen Biotech Art Co. Ltd., mouse CD47 monoclonal antibody (anti-CD47 mouse monoclonal antibody), purchased from Hangzhou Hua'an Biotechnology Co. Ltd., IFKine™ green donkey anti-mouse IgG antibody (IFKine™ green donkey anti-mouse IgG) was purchased from SubCoin Biotechnology Co. Ltd., HMGB1 *in situ* hybridization detection kit was purchased from Wuhan Dr. Cheng Co. Ltd., ATP content test kit was purchased from Beijing Solaibao Technology Co. Ltd.

Instruments:

Culture plate, culture bottle, culture dish (Corning Company, United States of America (USA)); optical microscope, fluorescence microscope (Olympus, Japan); low-speed centrifuge (China LC-4012); Carbon dioxide (CO_2) incubator (Thermo Fisher Scientific, Germany); constant temperature water bath (HH-W420, China); biosafety cabinet (Heal Force, China); pipette gun (Eppendorf, Germany); full-wavelength microplate reader (Thermo Fisher Scientific, Germany); flow cell sorting analyzer (BD FACSC Calibur, USA); high speed and low temperature centrifuge (FRESCO 17, Germany); high temperature and low speed centrifuge (Thermo Fisher Scientific, Germany); mini centrifuge, medical centrifuge and automatic pressure steam sterilization cooker (ZealWay, China).

Cell culture:

MC-3 cells were cultured in DMEM/F-12 complete medium (containing 10 % serum, 1 % penicillin-

streptomycin-gentamicin tri-antibody) and routinely cultured in an incubator containing 5 % CO_2, temperature 37°.

CCK-8 assay:

CCK-8 assay measured the cellular activity of ZER against MC-3. Cells in the growth log phase were seeded into 96-well plates for 24 h at a density of 5×10^4/ml, inoculum of 100 µl per well. Set concentration ZER concentration gradient 10, 20, 30, 40, 50 and 100 µmol/l, respectively in the microplate reader at 450 nm, wavelength detection 24 h, 48 h, 72 h and absorbent value (Optical Density (OD) value). Cell proliferation inhibition was calculated from the measured OD value (%)=(control-drug well)/(control-blank)×100 %. In addition, the final concentration of PTX was 10 % peak plasma concentration i.e., 360 ng/ml, and half was applied on epidermoid mucoid carcinoma cells after 48 h inhibition ratio[19].

Cell scratch assay to detect the effects of ZER and PTX on MC-3 migration:

Before the experiment, three lines behind the 6-well plate were drawn with a marker. Cells in the log growth phase were seeded into 6-well plates at a density of 5×10^4/ml, set blank control group, PTX group, ZER group and ZER+PTX drug combination group (this group was used in subsequent experiments). Draw a scratch line with the head perpendicular to the three parallel lines. Pictures were collected for 0 h, 24 h and 48 h under the microscope to calculate the cell migration area of each group.

Cell cure rate=(1-measured area /0 h area)×100 %

Apoptosis kit was used for ZER and PTX against MC-3 and apoptosis:

Cells in the log growth phase were seeded into 6-well plates at a density of 5×10^4/ml, after four groups treated with equal volume of drug, the supernatant were centrifuged and discarded, the cells of each group were resuspended with binding buffer, and Annexin V-FITC and PI dye solution were added. By flow cytometry, Annexin V-FITC underwent FL1 channel detection, and PI underwent FL2 channel detection.

CRT and CD47 expression were detected by immunofluorescence double staining:

Sterile cover slides were taken in 6-well plates, and the cells in the log growth phase were seeded into cover slides and cultured. After four groups with equal volume of drug treatment, the cells were fixed with paraformaldehyde and goat serum was blocked. Rabbit CRT monoclonal antibody (1:200) and mouse CD47 monoclonal antibody (1:200) were incubated in incubator for 1 h, washed in PBS, added Alexa Fluor 594, labeled sheep anti-rabbit IgG (H+L) antibody (1:200) and IFKine™ green donkey anti-mouse IgG antibody (1:200), incubated in incubator for 1 h (protected from light). In PBS, 4′,6-Diamidino-2-Phenylindole (DAPI) dye solution was added after washing. After washing with PBS, the coverslips were placed on the slides, dried and closed before observation under a microscope. The mean fluorescence intensity was analyzed and determined.

CRT and CD47 expression was determined by flow cytometry:

After the log growth phase cells were seeded into 6-well plates and treated with four groups with equal volume of drug, the cells were centrifuged and resuspended three times in PBS. Rabbit monoclonal antibody (1:200) and mouse CD47 monoclonal antibody (1:100) were added in an incubator for 1 h, and Alexa Fluor 488 labeled sheep anti-rabbit IgG (H+L) antibody (1:100) was added IFKine™ green donkey anti-mouse IgG antibody (1:100) and incubated in an incubator for 1h (protected from light), PBS was washed, centrifuged and resuspended to a flow tube for machine detection. The positive expression rates were determined separately. The ATP content was detected by the ATP bioluminescence kit.

Cells in growth log phase were seeded and cultured in 96-well plates, treated with equal volume drug, centrifuged, the supernatant was collected, placed in a low-speed centrifuge, and the supernatant was collected again at 1200 revolutions per minute (rpm) for 5 min. After the addition of the extract, the supernatant was collected by centrifugation at 10 000 ×g at 4° for 3 min, the working solution was added, and after fully mixing, 10 µmol/ml ATP standard was placed with each experimental group.

In the 96th well, the absorbance at 10 s at 340 nm was immediately in a microplate reader, as indicated ATP content was calculated. The HMGB1 expression was detected by a HMGB1 *in situ* hybridization detection kit.

An oligonucleotide probe for HMGB1 was used, and

HMGB1 expression was detected after digoxigenin labeling. The sterile cover slides were taken in 6-well plates, and the cells in the log growth phase were seeded into the cover slides for culture, treated with equal volume of drugs, and fixed with paraformaldehyde. Nucleic acid fragments were exposed with pepsin diluted with 3 % citrate and fixed after exposure. After washing with distilled water, pre-hybridization solution was added dropwise and incubated in an incubator for 4 h. After absorbing the excess liquid, the hybrids was added and incubated in an incubator overnight. After hybridization, the cells were washed with Saline-Sodium Citrate (SSC), 37° for 60 min of blocking solution, 37° for 60 min of biotinylated mouse anti-digoxigenin labeling in PBS, 37° for 20 min DAB, fully washed after color development. The cover slips were placed on the slides, dried and closed, and observed under a microscope. The mean positive expression of HMGB1 was determined.

Statistical methods:

The data obtained from the experiments were analyzed with Statistical Package for the Social Sciences (SPSS) 26.0 and GraphPad Prism 9.0 software, all experiments were repeated in triplicate, and the statistical methods including univariate analysis were analyzed by Analysis of Variance (ANOVA), student t-test, multiple comparisons between groups using Student-Newman-Keuls (SNK) method, test level $\alpha=0.05$, $p<0.05$.

RESULTS AND DISCUSSION

The inhibition of ZER increased significantly at 48 h ($p<0.01$), and at 48 h, ZER inhibited MC-3 at concentration dependence ($p<0.01$), and ZER at 40 µmol/l inhibited MC-3 growth by half-maximal Inhibitory Concentration (IC_{50}); the inhibition was more obvious at 72 h ($p<0.01$). Since DAMPs was exposed in early and medium stages at the time of ICD, 48 h was chosen as the optimal time of action for ZER and 40 µmol/l as the optimal experimental concentration for ZER (fig. 1). In addition, the final concentration of PTX was 10 % peak plasma concentration i.e., 360 ng/ml, and half of the inhibition rate was achieved after 48 h in mucoepidermoid cancer cells[20].

Comparing the cure rates of ZER, PTX and ZER+PTX groups. After 24 h and 48 h, cell migration gradually decreased (fig. 2). Cell migration in each experimental group at 24 h was statistically significant compared with the control group ($p<0.05$), and there was no difference between the dosing groups. By 48 h, the migration degree was decreased in the PTX group and the combined ZER+PTX group compared with the ZER group ($p<0.05$) (fig. 2).

The quadrant apoptotic plot shows that early and late apoptotic cells are concentrated in the lower and upper right regions. The results showed that ZER and PTX for 48 h, and the apoptosis rate gradually increased (fig. 3), the total apoptosis rate was higher than the control group ($p<0.01$), and the apoptosis rate was higher than the ZER group ($p<0.01$).

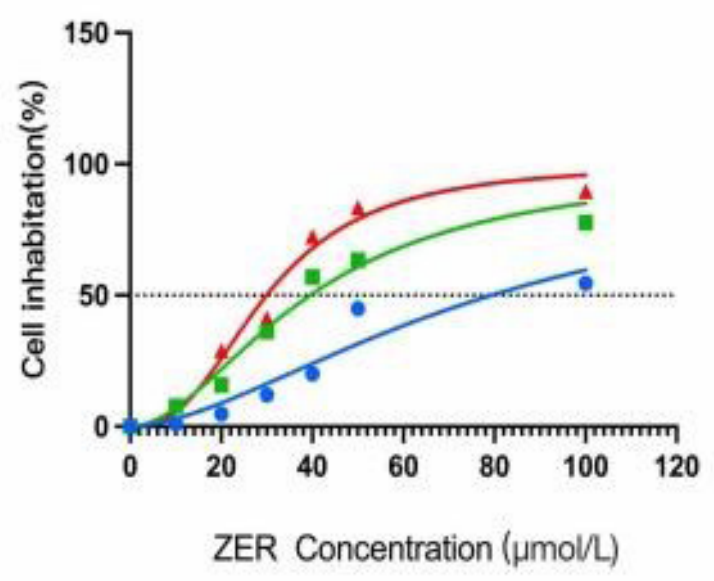

Fig. 1: The inhibition of MC-3 proliferation by different concentrations of ZER after 24 h, 48 h and 72 h of effect
Note: (●): 24 h; (■): 48 h and (▲): 72 h

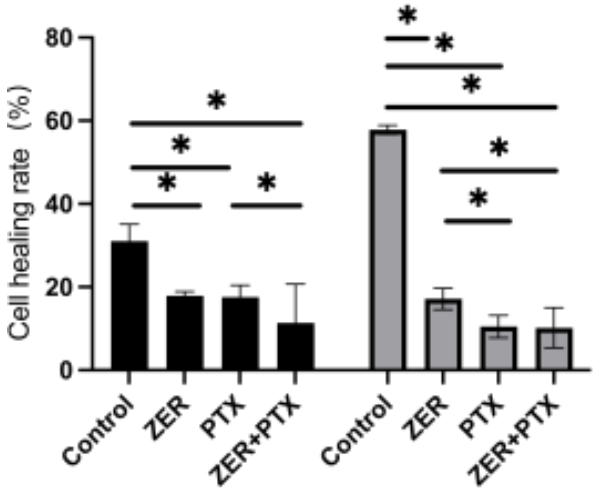

Fig. 2: Inhibition of MC-3 migration after 24 h and 48 h of ZER and PTX effects (40X)
Note: *p<0.05, for each drug addiction group compared with the control group, (■): 24 h and (▭): 48 h

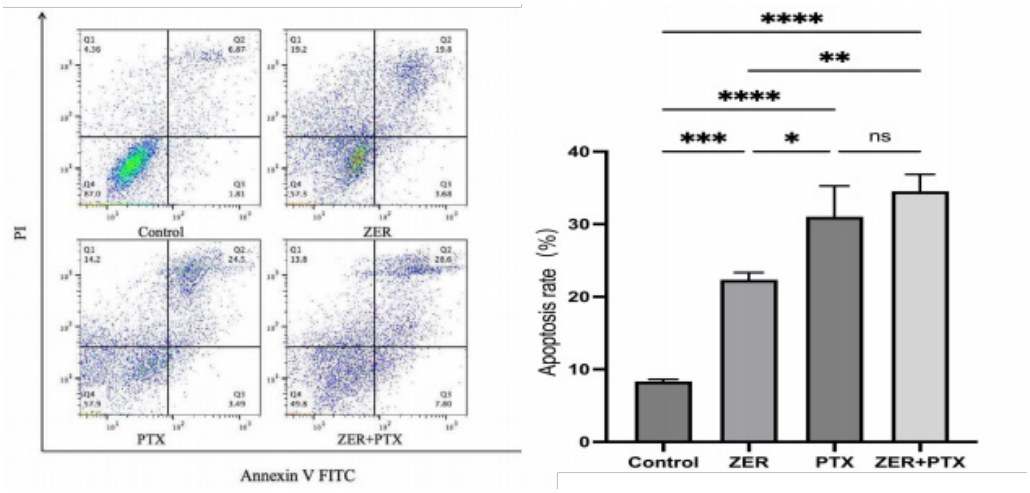

Fig. 3: Promotion of MC-3 apoptosis by ZER and PTX after 48 h of effects
Note: *p<0.05, **p<0.01, ***p<0.001, ****p<0.0001 and ^{ns}p>0.05

Immunofluorescence results showed that the expression of green fluorescent CD47 was reduced in each drug group compared with control group respectively (p<0.05); the red fluorescence CRT expression in each group increased and the difference in mean cell fluorescence intensity was statistically significant (p<0.05), and the difference compared with combination alone (p<0.05) (fig. 4).

The results of CRT expression by flow cytometric technology showed that the CRT peak in the dosing group compared with control. Statistical analysis showed that the difference between each drug addiction group and control group was statistically significant (p<0.01), and the difference between groups was statistically significant (p<0.05), i.e., the combination group could enhance the CRT expression of MC-3 cells. For CD47 expression, CD47 expression was high in the control group, and the CD47 peak was shifted to the left compared with control. Statistical analysis showed that the difference between each drug addiction group and the control group was statistically significant (p<0.01), and compared with the combination group alone (p<0.05) (fig. 5).

Analysis of DAB staining, HMGB1 showed positive expression of brown fluorescence and increased in the dosing group compared with the control group was apparent by ImageJ analysis.

Here, under DAB staining, mean HMGB1 positive density was compared to control (p<0.01) and combination expression compared to drug alone (p<0.01). As determined by the ATP bioluminescence kit, the results showed that the ATP content was statistically significant compared to control (p<0.05). And the combination group compared with ATP content alone (p<0.01) (fig. 6).

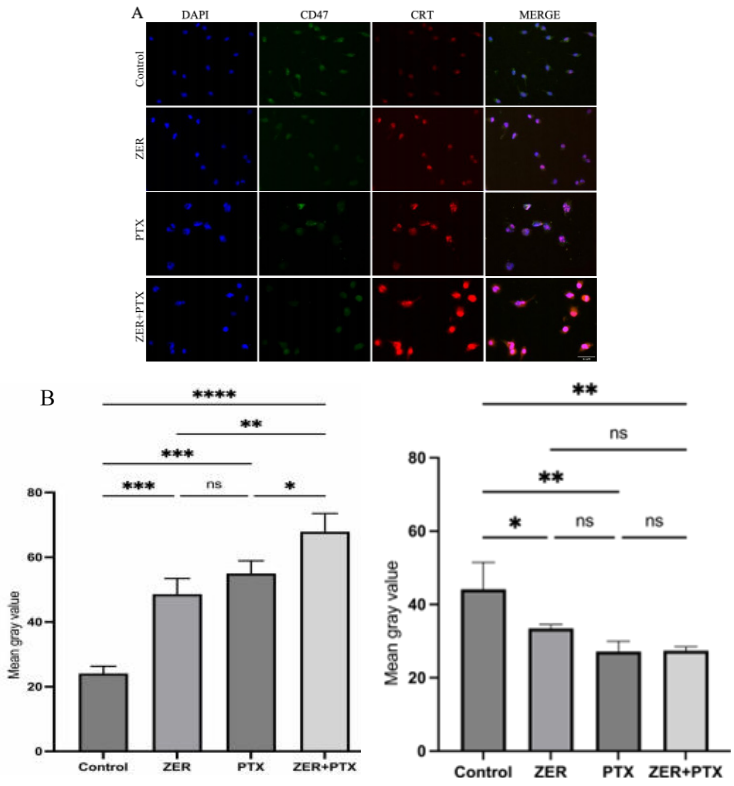

Fig. 4: The expressions of CRT and CD47 detected by immunofluorescence after ZER and PTX induced ICD in MC-3, (A): The expression of CD47 and CRT (400X) was observed under fluorescence microscope, green represents CD47 with a weakening trend and red represents CRT with an enhancement trend and (B): Mean cellular fluorescence intensity of CRT, with an enhancement trend CD47 mean cellular fluorescence intensity, weakened in each drug addiction group compared with the control group
Note: *p<0.05, **p<0.01, ***p<0.001, ****p<0.0001 and ^{ns}p>0.05

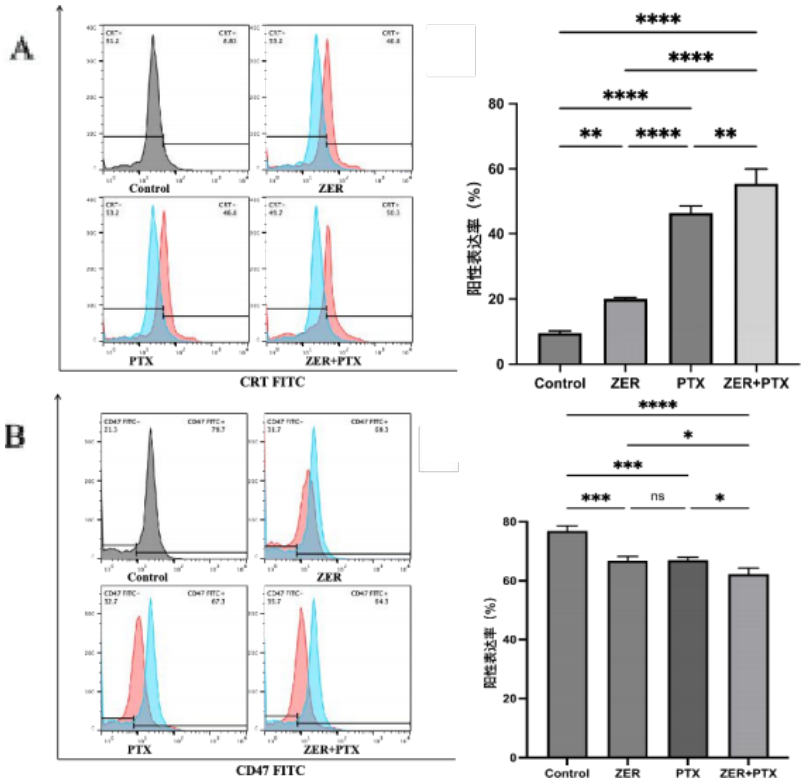

Fig. 5: The expressions of CRT and CD47 detected by flow cytometry after ZER and PTX induced ICD in MC-3, (A): The expression and positive expression rate of CRT were detected by flow cytometry and (B): The expression and positive expression rate of CD47 were measured by flow cytometry and decreased compared with control
Note: *p<0.05, **p<0. 01, ***p<0.001, ****p<0.0001 and ^{ns}p>0.05

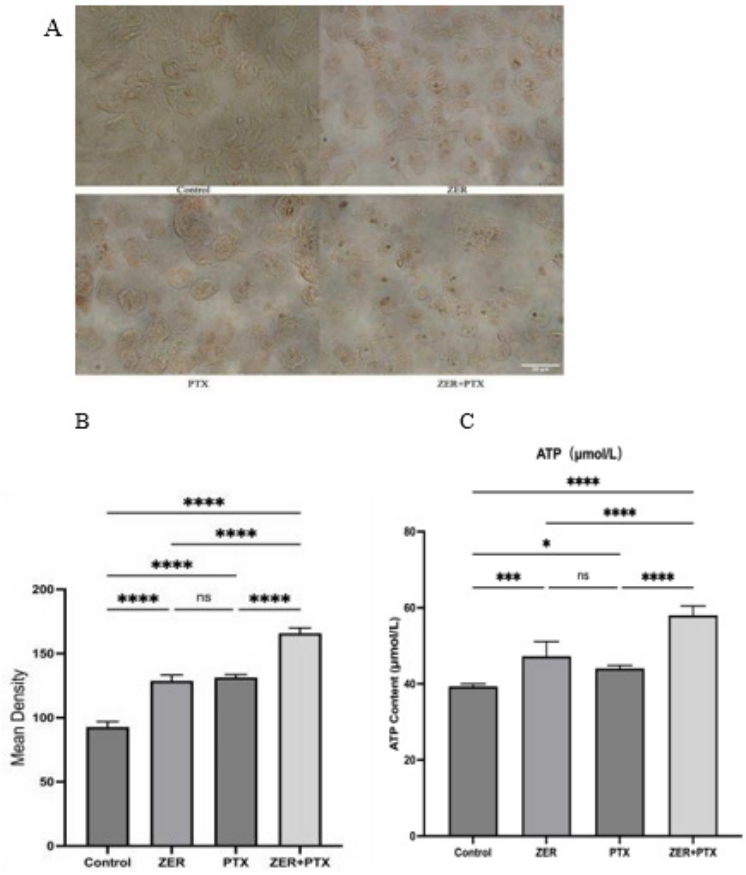

Fig. 6: The effects of release of HMGB1, ATP after ICD induced in MC-3 by ZER and PTX, (A): The expression of HMGB1 was detected by *in situ* hybridization, and the brown fluorescent fraction represents the expression of HMGB1 (400X); (B): *In situ* hybridization showed enhanced HMGB1 expression compared with control and (C): The ATP bioluminescence kit detected more ATP content as compared with control
Note: *p<0.05, **p<0.01, ***p<0.001, ****p<0.0001 and nsp>0.05

All cancer cells show abnormal cell proliferation, and recent studies have been increasingly confirmed that abnormal tumor energy metabolism and escape the monitoring of the immune system become a common property of tumors[21]. To suppress the immune escape properties of tumors, clinical immunotherapy can be solved by inducing ICD. In the microenvironment of the tumor, ICD, tumor cells expose DAMPs and attract antigen presentation; presenting receptors or ligands on cell Dendritic Cells (DC), thus activating immature DC to transform into mature DC. Mature DC exert antigen-presenting effects to stimulate the characteristic T cell response, thus allowing the phagocytes to exert phagocytosis to kill more tumor cells[12]. Therefore, the effort to find a low cytotoxic inducer with weak effect on normal tissues has become a hot topic. Currently, chemo radiotherapy and photodynamic therapy can activate tumorigenesis ICD, and among different inducers, natural compounds attract much attention due to their low toxicity and by inhibiting various pathways involved in cancer development. Studies have found that natural compounds can change the microenvironment of immunosuppressive tumors, and induce ICD when used with chemotherapy drugs or alone, and natural compounds have the potential to increase anticancer immunotherapy[14]. ZER has shown great potential in a variety of diseases. Compared with the effect of cytotoxic effect on cancer cells, ZER has little effect on normal cells. The properties of ZER include anti-inflammatory, anti-aging agents, anti-atherogenic, antibacterial, and hepatoprotective activities. In terms of anti-tumor, the main functions of ZER include inhibition of tumor proliferation activity and reversal of tumor multidrug resistance[22-27]. The terpenoid PTX, also derived from natural plants, has become a commonly used chemotherapy drug for salivary gland tumors. Due to its poor water solubility, not easy to remove and excessive accumulation in peripheral nerves is easy to produce toxicity, PTX is rarely given as monotherapy and can enhance its anti-tumor activity when combined[28,29]. While the facial nerve and its branches are distributed around the salivary glands,

symptoms such as facial neurotoxicity are more likely to occur when PTX is treated for salivary gland tumors. Therefore, from the salivary gland tumors and the anti-tumor properties of glutathione, we revealed that glutathione can promote apoptosis and inhibit its proliferation and migration, and induce ICD of MC-3, and its combination with PTX can enhance its effect.

In the early stages of ICD, CRT is rapidly transferred from the Endoplasmic Reticulum (ER) to the surface of the cell membrane. CRT, which appears on the tumor cell membrane, acts as a "phagocytosis" signal, recognized and bound by the specific receptor CD91 on DC, thus presenting to cytotoxic T lymphocytes Cytotoxic Lymphocyte (CTL) that are phagocytosed by phagocytes[30]. Inactivation of CRT by means of inhibiting the expression or gene knockout of CRT can lead to loss of immunogenicity of tumor cells, and when genes expressing CRT continue to recombine in CRT, tumor cells continue to undergo immunogenic death. Therefore, ER, stress-mediated translocation of CRT is essential for the development of ICD. It was found that eukaryotic Initiation Factor-2 Alpha (eIF2α) phosphorylation caused by the eukaryotic cell eIF2α kinase is necessary for CRT translocation[31]. During ER stress, eIF2α is phosphorylated in response to receiving external stimuli and accompanies the termination of translation of related proteins. Proapoptotic cysteine-3 (caspase-3) and cysteine-8 are activated, and the ER proteins are hydrolyzed. Meanwhile, the proapoptotic B cell lymphoma-2 (Bcl-2) family members Bcl-2-Associated X Protein (BAX) and Bcl-2 Antagonist Killer 1 (BAK) accumulate in the mitochondrial outer membrane mediated by Synaptosome-Associated Protein 25 (SNAP25), and CRT is smoothly transmitted from the ER to the Golgi apparatus and is expressed on the cell surface through CRT-containing cytoplasmic vesicles[32]. Thus, eat-me signals are generated on the membrane surface, accompanied by the massive release of proinflammatory cytokines such as Tumor Necrosis Factor-Alpha (TNF-α) and Interleukin-6 (IL-6). The anti-tumor immune response is constantly enhanced[15]. CD47 is an innate immune checkpoint for cellular immune response. In tumor cells, CD47 is highly expressed to escape the immune response and thus avoid the clearance of phagocytes. CD47 binds with ligand Signaling Regulating Protein Alpha (SIRPα), and the CD47-SIRPα axis shows enhanced inhibition of macrophage cell-mediated phagocytosis, which causes cellular immune escape[33,34]. The results of this study showed that ZER, PTX, were able to inhibit the expression of CD47, but the degree of inhibition was not significant with the combination. Related studies showed that SIRPα is highly expressed in DC and phagocytes, and blocking the CD47-SIRPα axis is more effective in inhibiting tumor immune escape[35]. Therefore, the subsequent in-depth research needs to explore the mechanism with the co-culture experiments of macrophages and animal experiments. In conclusion, when ICD occurs, the swallow me and do not swallow me signals appear to fade, allowing the cells undergoing ICD to be effectively recognized by DC and phagocytosed by macrophages.

ATP is an important component of the tumor microenvironment, and a large amount of ATP is released by the autophagy of the tumor cells. Autophagy is considered as a premortem stress adaptation mechanism that can degrade cytosolic proteins, aggregates and damaged organelles through catabolic processes. During its degradation, the fusion of the auto phagosome-lysosome complex and of the lysosome to the plasma membrane ultimately leads to the release of ATP and constitutes the main source of extracellular ATP release by the intracellular environment[36].

In the process, ATP binds to the purinergic receptors P2RY2 and P2RX7 expressed on the tumor surface, causing potent chemotaxis to dendritic cells and their precursors. In addition, P2RX7 signaling also activates the NOD-Like Receptor Protein 3 (NLRP3) inflammasome, which then triggers the release of the inflammatory cytokine IL-1β involved in the anti-tumor immune response[37]. Thus, tumor-thin, cellular-released extracellular ATP acts as a find-me signal with the dual role of recruitment, activation of DC and inflammatory pathways[38]. HMGB1 is a highly conserved nuclear protein and HMGB1 is largely released outside the cell when cells are in a dying state[39]. In response to the ICD of tumor cells, HMGB1 is released outside the cell to bind to the Pattern Recognition Receptor (PRR),

This includes the Toll-Like Receptor 4 (TLR4) and the Receptor for Advanced Glycation End products (RAGE). Notably, TLR 4 is mainly expressed on DC, and after TLR4 recognizing HMGB1 triggers the major Myeloid Differentiation factor (MyD) 88. TLR4/MyD 88 pathway enhances the processing of tumor-related antigen Tumor-Associated Antigen (TAA) by inhibiting the fusion between phagosomes and lysosomes, thus activating monocytes or

macrophages to release proinflammatory cytokines, and inducing DC maturation to enhance the antigen presentation of DC to promote tumorigenesis ICD[40].

Tumor cells in CD lack HMGB1 and expression impairs DC mediated TAA, priming of effector T cells[41]. Based on *in vitro* experimental studies, this study revealed that ZER can promote the apoptosis of MEC of salivary glands and inhibit its proliferation and migration, enhance the effect in combination with PTX, and induce the immunogenic death of MEC cells by affecting the changes in damage-related molecular patterns. The combination of ZER and litaxol can enhance the expression of CRT, enhance the release of high mobility group proteins HMGB1 and ATP, and then enhance the immunogenic death of mucoepidermoid cancer cells.

In this study, through the combination of ZER and PTX in mucoepiderid cancer cells, we further explored the further study of various pathways and *in vitro* animal experiments, and the targeted activation of ICD for the treatment of salivary gland tumors has important scientific significance and practical value to provide reliable data to support the survival and prognosis of patients with MEC.

Authors' contributions:

Guixin Li and Pengcheng Huang have contributed equally to this work and share first authorship.

Funding:

This study was supported by Provincial Science and Technology Plan Project of Sichuan Provincial Science and Technology Department (No: 2022SNZY001); Science and Technology Project of Sichuan Provincial Health Commission (Suitable Technology Base) (No: 2022JDXM021); Key project of Sichuan Grassroots Health Development Research Center (No: SWFZ20-C-086); Western Stomatology Clinical Research Foundation Project of Chinese Stomatological Association (No: CSA-W2023-03) and General Project of Sichuan Administration of Traditional Chinese Medicine (No: 2021MS100).

Conflict of interests:

The authors declared no conflict of interests.

REFERENCES

1. Alsanie I, Rajab S, Cottom H, Adegun O, Agarwal R, Jay A, *et al*. Distribution and frequency of salivary gland tumours: An international multicenter study. Head Neck Pathol 2022;16(4):1043-54.
2. Skalova A, Hyrcza MD, Leivo I. Update from the 5th edition of the World Health Organization classification of head and neck tumors: Salivary glands. Head Neck Pathol 2022;16(1):40-53.
3. Schwarz S, Stiegler C, Muller M, Ettl T, Brockhoff G, Zenk J, *et al*. Salivary gland mucoepidermoid carcinoma is a clinically, morphologically and genetically heterogeneous entity: A clinicopathological study of 40 cases with emphasis on grading, histological variants and presence of the t (11;19) translocation. Histopathology 2011;58(4):557-70.
4. Yih WY, Kratochvil FJ, Stewart JC. Intraoral minor salivary gland neoplasms: Review of 213 cases. J Oral Maxillofacial Surg 2005;63(6):805-10.
5. Mendenhall WM, Morris CG, Amdur RJ, Werning JW, Villaret DB. Radiotherapy alone or combined with surgery for salivary gland carcinoma. Cancer 2005;103(12):2544-50.
6. Pfister DG, Spencer S, Adelstein D, Adkins D, Anzai Y, Brizel DM, *et al*. Head and neck cancers, version 2.2020, NCCN clinical practice guidelines in oncology. J Natl Compr Cancer Network 2020;18(7):873-98.
7. Gilbert J, Li Y, Pinto HA, Jennings T, Kies MS, Silverman P, *et al*. Phase II trial of taxol in salivary gland malignancies (E1394): A trial of the eastern cooperative oncology group. Head Neck 2006;28(3):197-204.
8. Raguse JD, Gath HJ, Bier J, Riess H, Oettle H. Docetaxel (Taxotere) in recurrent high grade mucoepidermoid carcinoma of the major salivary glands. Oral Oncol Extra 2004;40(1):5-7.
9. Suen JY, Johns ME. Chemotherapy for salivary gland cancer. Laryngoscope 1982;92(3):235-9.
10. Pires FR, de Almeida OP, de Araujo VC, Kowalski LP. Prognostic factors in head and neck mucoepidermoid carcinoma. Arch Otolaryngol Head Neck Surg 2004;130(2):174-80.
11. Sama S, Komiya T, Guddati AK. Advances in the treatment of mucoepidermoid carcinoma. World J Oncol 2022;13(1):1-7.
12. Birmpilis AI, Paschalis A, Mourkakis A, Christodoulou P, Kostopoulos IV, Antimissari E, *et al*. Immunogenic cell death, DAMPs and prothymosin α as a putative anticancer immune response biomarker. Cells 2022;11(9):1415.
13. Fucikova J, Kepp O, Kasikova L, Petroni G, Yamazaki T, Liu P, *et al*. Detection of immunogenic cell death and its relevance for cancer therapy. Cell Death Dis 2020;11(11):1013.
14. Amiri M, Molavi O, Sabetkam S, Jafari S, Montazersaheb S. Stimulators of immunogenic cell death for cancer therapy: Focusing on natural compounds. Cancer Cell Int 2023;23(1):200.
15. Xie D, Wang Q, Wu G. Research progress in inducing immunogenic cell death of tumor cells. Front Immunol 2022;13:1017400.
16. Kirana C, McIntosh GH, Record IR, Jones GP. Antitumor activity of extract of *Zingiber aromaticum* and its bioactive sesquiterpenoid zerumbone. Nutr Cancer 2003;45(2):218-25.
17. Lau TS, Chan LK, Man GC, Wong CH, Lee JH, Yim SF, *et al*. Paclitaxel induces immunogenic cell death in ovarian cancer *via* TLR4/IKK2/SNARE-dependent exocytosis. Cancer Immunol Res 2020;8(8):1099-111.
18. Zhu J. Preliminary investigation of the expression of CRT, HSP70, HMGB1, and ATP by allotinib hydrochloride and paclitaxel. Zunyi Med Univ; 2022.
19. Miao Y. Establishment of Mc3/5-FU and its biological properties. Fourth Military Med Univ; 2009.
20. Dong Q, Yang Y, Wu W. Experimental study of apoptosis induced by taxol in combination with tumor necrosis factor alpha in mucoepidermoid carcinoma cells. Beijing Stomatol 2008;5:260-2.
21. Fucikova J, Spisek R, Kroemer G, Galluzzi L. Calreticulin and

cancer. Cell Res 2021;31(1):5-16.
22. Girisa S, Shabnam B, Monisha J, Fan L, Halim CE, Arfuso F, *et al*. Potential of zerumbone as an anti-cancer agent. Molecules 2019;24(4):734.
23. Rahman HS, Rasedee A, Yeap SK, Othman HH, Chartrand MS, Namvar F, *et al*. Biomedical properties of a natural dietary plant metabolite, zerumbone, in cancer therapy and chemoprevention trials. Biomed Res Int 2014;2014(1):920742.
24. Zainal NS, Gan CP, Lau BF, San YP, Tiong KH, Rahman ZA, *et al*. Zerumbone targets the CXCR4-RhoA and PI3K-mTOR signaling axis to reduce motility and proliferation of oral cancer cells. Phytomedicine 2018;39:33-41.
25. Edagawa M, Kawauchi J, Hirata M, Goshima H, Inoue M, Okamoto T, *et al*. Role of Activating Transcription Factor 3 (ATF3) in Endoplasmic Reticulum (ER) stress-induced sensitization of p53-deficient human colon cancer cells to Tumor Necrosis Factor (TNF)-Related Apoptosis-Inducing Ligand (TRAIL)-mediated apoptosis through up-regulation of Death Receptor 5 (DR5) by zerumbone and celecoxib. J Biol Chem 2014;289(31):21544-61.
26. Schnoell J, Stanisz I, Jank BJ, Stanek V, Schmid R, Brunner M, *et al*. Zerumbone acts as a radiosensitizer in head and neck squamous cell carcinoma. Invest New Drugs 2022:1-8.
27. Kalesh KA, Clulow JA, Tate EW. Target profiling of zerumbone using a novel cell-permeable clickable probe and quantitative chemical proteomics. Chem Commun 2015;51(25):5497-500.
28. Zeng N, Zhao X, Zeng Y. Effect of fringerone on proliferation, apoptosis, invasion and migration capacity of human oral squamous carcinoma cells. J Lab Surg 2019;28(5):339-43.
29. Stage TB, Bergmann TK, Kroetz DL. Clinical pharmacokinetics of paclitaxel monotherapy: An updated literature review. Clin Pharmacokinet 2018;57(1):7-19.
30. Liu P, Zhao L, Kepp O, Kroemer G. Quantitation of calreticulin exposure associated with immunogenic cell death. Methods Enzymol 2020;632:1-13.
31. Azuma Y, Suzuki K, Higai K, Matsumoto K, Tada S. Biphasic increases of cell surface calreticulin following treatment with mitoxantrone. Biol Pharm Bull 2020;43(10):1595-9.
32. Panaretakis T, Kepp O, Brockmeier U, Tesniere A, Bjorklund AC, Chapman DC, *et al*. Mechanisms of pre-apoptotic calreticulin exposure in immunogenic cell death. EMBO J 2009;28(5):578-90.
33. Zhang W, Huang Q, Xiao W, Zhao Y, Pi J, Xu H, *et al*. Advances in anti-tumor treatments targeting the CD47/SIRPα axis. Front Immunol 2020;11:18.
34. Chao MP, Weissman IL, Majeti R. The CD47-SIRPα pathway in cancer immune evasion and potential therapeutic implications. Curr Opin Immunol 2012;24(2):225-32.
35. Wang YJ, Fletcher R, Yu J, Zhang L. Immunogenic effects of chemotherapy-induced tumor cell death. Genes Dis 2018;5(3):194-203.
36. Zhang Z, Chen G, Zhou W, Song A, Xu T, Luo Q, *et al*. Regulated ATP release from astrocytes through lysosome exocytosis. Nat Cell Biol 2007;9(8):945-53.
37. Sala A, Ferrari D, Corinti S, Cavani A, di Virgilio F, Girolomoni G. Extracellular ATP induces a distorted maturation of dendritic cells and inhibits their capacity to initiate T_h1 responses. J Immunol 2001;166(3):1611-7.
38. Ghiringhelli F, Apetoh L, Tesniere A, Aymeric L, Ma Y, Ortiz C, *et al*. Activation of the NLRP3 inflammasome in dendritic cells induces IL-1β-dependent adaptive immunity against tumors. Nat Med 2009;15(10):1170-8.
39. Chen R, Kang R, Tang D. The mechanism of HMGB1 secretion and release. Exp Mol Med 2022;54(2):91-102.
40. Shiratsuchi A, Watanabe I, Takeuchi O, Akira S, Nakanishi Y. Inhibitory effect of Toll-like receptor 4 on fusion between phagosomes and endosomes/lysosomes in macrophages. J Immunol 2004;172(4):2039-47.
41. Kroemer G, Kepp O. Radiochemotherapy-induced elevations of plasma HMGB1 levels predict therapeutic responses in cancer patients. Oncoimmunology 2021;10(1):2005859.

This article was originally published in a special issue, "Clinical Advancements in Life Sciences and Pharmaceutical Research" Indian J Pharm Sci 2024:86(5) Spl Issue "229-238"